REVISTA MATÉRIA V.30
ISSN 1517-7076 articles e20240987, 2025

Enhancing durability and sustainability of foamed concrete: Predictive modeling and multivariate analysis of slag-based material substitutions

Vijayaraghavan Jagadeesan[1], Vairamani Gopal[2], Thivya Jagadeesan[3]

[1]University College of Engineering Ramanathapuram, Department of Civil Engineering. Ramanathapuram, Tamil Nadu, India.
[2]Thiagarajar Polytechnic College, Department of Civil Engineering. Salem, Tamil Nadu, India.
[3]University College of Engineering Dindigul, Department of Civil Engineering. Dindigul, Tamil Nadu, India.
e-mail: drjvr1988@gmail.com, gvairamani2015@gmail.com, thivyame@gmail.com

ABSTRACT

This study presents a novel, data-driven approach to enhancing the durability and sustainability of foamed concrete through the strategic incorporation of ultrafine slag (UFS) as a partial cement substitute and crushed steel slag (CSS) as a partial sand replacement. A total of 72 foamed concrete mixes were prepared by varying foam content (20–80 kg/m^3), UFS (0–50% of cement), and CSS (0–50% of sand) levels. The density of the hardened foamed concrete ranged from 1450 to 1750 kg/m^3, with higher foam content contributing to lower densities due to increased air voids. The study evaluated porosity and chloride diffusivity as primary durability indicators, measured according to ASTM C642 and ASTM C1202, respectively. Results show that increasing UFS from 0% to 50% reduced porosity by up to 6% (from 16.5% to 10.5%) and improved compressive strength by 10 MPa at low foam contents. However, these benefits diminished at higher foam content. CSS, while beneficial from a sustainability standpoint, slightly increased porosity and chloride diffusivity due to its irregular shape. Predictive modeling using an Artificial Neural Network (ANN) outperformed ANOVA in accuracy (R^2 > 0.95), capturing non-linear relationships among the variables.

Keywords: Ultrafine Slag; Foamed Concrete; Sustainability; Artificial Neural Network (ANN); Porosity.

VISUAL ABSTRACT

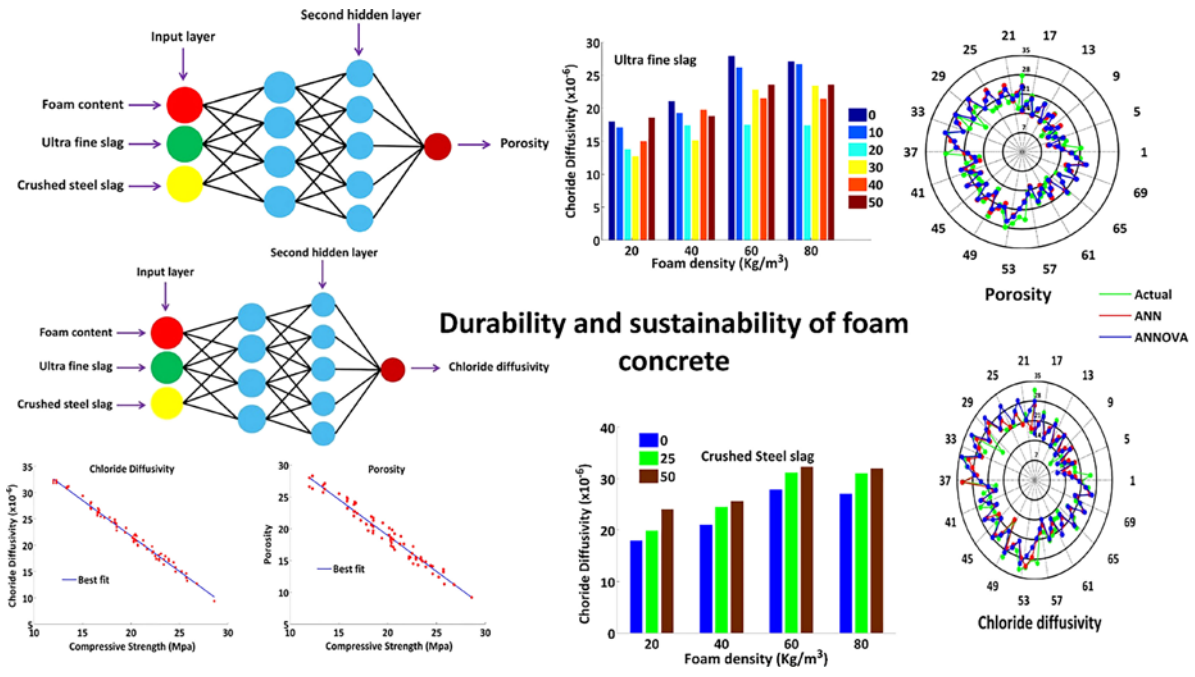

Corresponding Author: Vijayaraghavan Jagadeesan Received on 31/12/2024 Accepted on 12/09/2025

DOI: https://doi.org/10.1590/1517-7076-RMAT-2024-0987

1. INTRODUCTION

Foamed concrete, a class of lightweight cellular concrete, has gained considerable traction in the construction industry due to its favorable properties such as reduced density, thermal insulation, sound absorption, and ease of handling [1, 2]. Unlike conventional concrete, foamed concrete incorporates a high volume of stable air bubbles, which results in densities typically ranging between 300 and 1800 kg/m^3. These properties make it a desirable material for a wide range of applications, such as thermal insulation layers, trench reinstatement, void filling, prefabricated panels, and lightweight structural components in multi-storey buildings [3].

Despite its promise, foamed concrete has historically been limited to non-structural applications. The primary reason is its reduced mechanical strength and limited long-term durability, both of which are highly sensitive to foam volume and pore structure [4]. The high air content, while beneficial for weight reduction and insulation, leads to increased porosity, which in turn reduces compressive strength and makes the concrete vulnerable to permeability-related deterioration such as chloride ingress, carbonation, and freeze-thaw damage [5, 6].

In light of modern sustainability goals and increasing urbanization, there is a growing demand for high-performance, environmentally friendly construction materials. The use of industrial by-products, such as ultrafine slag (UFS) and crushed steel slag (CSS), presents a dual advantage—enhancing the engineering properties of concrete while simultaneously addressing the issues of resource depletion and industrial waste disposal [7–9].

1.1. Role of ultrafine slag (UFS) and crushed steel slag (CSS)

Ultrafine slag, produced as a by-product of blast furnace operations in steel manufacturing, is rich in calcium, silica, and alumina and exhibits high pozzolanic activity due to its fine particle size [10, 11]. When used as a partial replacement for cement, UFS not only contributes to strength development through secondary hydration reactions but also improves the concrete microstructure by filling capillary pores, thereby reducing permeability and enhancing durability [12, 13]. Recent studies have shown that the incorporation of UFS can reduce porosity by up to 30% and increase strength by 15–20% in traditional concrete systems [14, 15].

Crushed steel slag (CSS), on the other hand, is a granular material obtained from the solidification and processing of molten slag during steel production. While its use as a fine aggregate replacement in concrete is still under development, CSS offers significant environmental benefits by reducing the extraction of natural sand, which is becoming increasingly scarce and environmentally regulated [16, 17]. Its rough texture and high angularity enhance mechanical interlocking, although it can disrupt packing density if not graded properly. Prior work has shown mixed results: some studies reported increased compressive strength due to improved bond characteristics, while others noted increased porosity due to poor matrix compaction [18, 19].

1.2. Recent developments in lightweight and foamed concretes

Over the past decade, several research initiatives have focused on improving the performance of lightweight concrete using alternative materials. For instance, GANAPATHY *et al*. [20, 21] investigated the effects of fly ash and silica fume in porous concrete and observed improvements in strength and alkalinity stability. Similarly, KADHAR *et al*. [22] explored the optimization of self-compacting concrete using lightweight aggregates, aiming to balance flow and durability. More specifically, studies like “Chlorine salt influence on durability and strength of additive-free EPS lightweight concrete” and “Evaluation of fracture mechanics parameters of lightweight concrete by implementing natural pumice stone as coarse aggregate” have demonstrated that chloride exposure and aggregate morphology play a vital role in the microstructural behavior and fracture resistance of lightweight concretes.

While these contributions are significant, most of these works focus on either strength or durability but not both. Moreover, the combined effect of foam volume, UFS, and CSS on the porosity and chloride resistance of foamed concrete remains underexplored, particularly when analyzed using robust statistical and predictive modeling tools.

1.3. Limitations in existing research

A comprehensive review reveals several limitations in the current literature:

- Most studies focus on single-variable substitutions (either cement or aggregate) without evaluating interactions between multiple substitutions [23, 24].
- There is limited integration of machine learning tools for predictive performance modeling in concrete design. Predictive models such as artificial neural networks (ANN) are rarely applied to foamed concrete systems, despite their proven success in other civil engineering applications [25].

- The density and durability trade-off is not quantitatively addressed. While foamed concrete aims to be lightweight, the direct impact of mix proportions on hardened density, porosity, and strength has not been clearly mapped out [26, 27].
- Prior studies often lack standardized testing in accordance with ASTM methods for porosity and chloride diffusivity, which limits the reliability and international applicability of their conclusions [27–38].

1.4. Research gap and problem statement

While prior research has acknowledged the individual benefits of UFS and CSS in concrete systems, there is a clear research gap in understanding their combined influence in the context of foamed concrete durability, particularly under varying foam contents. No systematic study has yet quantified how foam-induced porosity interacts with SCM-based matrix densification or how to balance these effects to optimize both mechanical performance and sustainability.

Furthermore, there is a lack of predictive tools that can forecast the durability performance (e.g., porosity and chloride diffusivity) of foamed concrete based on mix variables, which hampers efficient mix design and widespread field implementation.

1.5. Objectives and novelty of the study

The present study aims to bridge these gaps by

1. Investigating the influence of ultrafine slag and crushed steel slag on porosity, strength, and chloride diffusivity of foamed concrete at varying foam contents (20–80 kg/m^3).
2. Quantifying hardened density, porosity, and chloride diffusivity using standardized ASTM C642 and C1202 procedures, enabling international benchmarking.
3. Applying artificial neural networks (ANN) alongside ANOVA to model and predict durability indicators, capturing both linear and nonlinear relationships in multivariate data.
4. Design of optimal mix strategies to maximize durability while maintaining lightweight properties, contributing to sustainable concrete design.

1.6. Significance and global relevance

By combining experimental, statistical analysis, and machine learning, this research provides a novel and holistic methodology for developing eco-efficient foamed concrete systems. The findings are relevant for developing nations focused on durable infrastructure and low carbon as well as advanced economies aiming to reuse industrial waste in green construction. Moreover, the results contribute to ongoing global efforts such as the UN Sustainable Development Goals (SDG 9 and SDG 12) by promoting innovation, resource conservation, and sustainable industrial practices. By employing ANN, this study models the complex interactions between the constituent materials of foamed concrete and predicts the resultant properties based on the varied compositions. ANOVA, on the other hand, helps in identifying the significant differences in durability characteristics caused by different replacement levels of ultrafine slag and crushed steel slag. This dual approach not only enhances the accuracy of the predictions but also provides a deep understanding of the material's behavior under different compositional changes.

2. MATERIALS AND METHODS

2.1. Materials

The materials used in this study were Ordinary Portland Cement (OPC) conforming to IS 12269:2013, ultrafine slag (UFS), crushed steel slag (CSS) as fine aggregate replacement, natural river sand, synthetic foaming agent, and potable water. The mix design was developed with a constant water-to-cement ratio (w/c) of 0.5 across all combinations to ensure comparability. The chemical composition of ultrafine slag was determined using X-ray fluorescence (XRF) analysis (ASTM C114), ensuring accuracy in oxide quantification. The average particle sizes of OPC (12.4 μm) and UFS (3.8 μm) determined via laser diffraction.

The ultrafine slag, sourced as a by-product of steel production, exhibited high pozzolanic activity. Its chemical composition is presented in Table 1. It was used as a partial replacement for cement at levels of 0%, 10%, 20%, 30%, 40%, and 50% by weight.

Crushed steel slag was used to replace sand at 0%, 25%, and 50% by weight. The CSS was sieved to match the particle size distribution recommended in ASTM C33/C33M-18, which defines the upper and lower limits for fine aggregates. The gradation curves of both the river sand and CSS were plotted and compared with

ASTM-recommended limits, confirming acceptable compliance. The fineness modulus of sand and CSS were found to be 2.69 and 3.15, respectively (Figure 1).

A commercial synthetic foaming agent was used to create stable pre-formed foam. Foam contents were varied at 20 kg/m^3, 40 kg/m^3, 60 kg/m^3, and 80 kg/m^3. The foam was generated using a calibrated foaming machine and measured by weight using a digital scale with ±0.1 g accuracy (Table 2; Figure 2).

2.2. Mix proportion design

The mix design is structured as a factorial design using the following. A Foam Content: 20, 40, 60, and 80 kg/m^3. Ultra-Fine Slag Replacement of 0%, 10%, 20%, 30%, 40%, and 50% by weight of cement. Crushed Steel Slag Replacement of 0%, 25%, and 50% by weight of sand. This design results in multiple mix combinations, each aimed at achieving different mechanical and flow properties. The Design of Experiments (DOE) approach helps reduce the number of experimental trials needed to capture the significant interactions between variables, using a factorial model that assesses all possible combinations within the range of input parameters. A total of 72 mixes were designed following the factorial DoE. Representative mixes are shown in Table 3.

Table 1: Chemical constituent of Ultra-fine slag.

CHEMICAL CONSTITUENT	% BY MASS
CaO	33
$A1_20_3$	18
Fe_20_3	1.9
SiO_2	30
MgO	9
SO_3	0.5

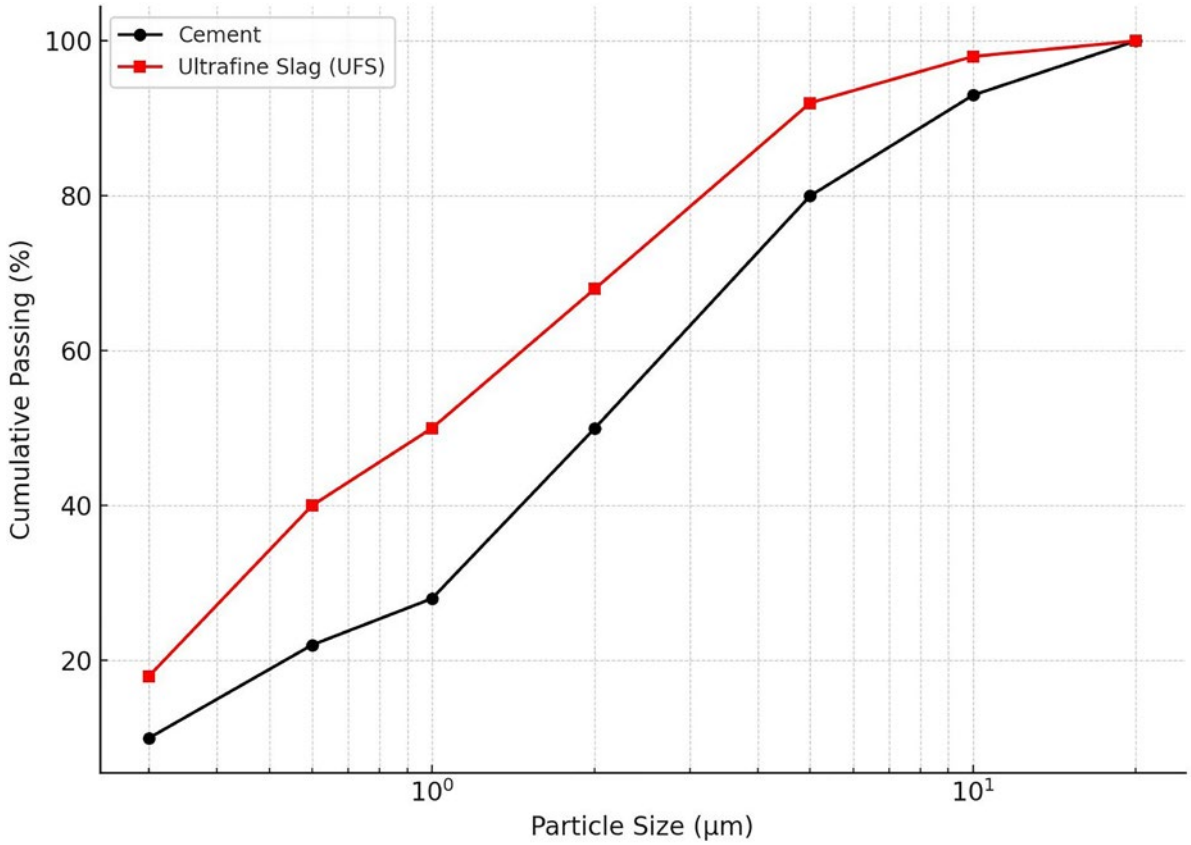

Figure 1: Particle size distribution curve of cement and ultra fine slag.

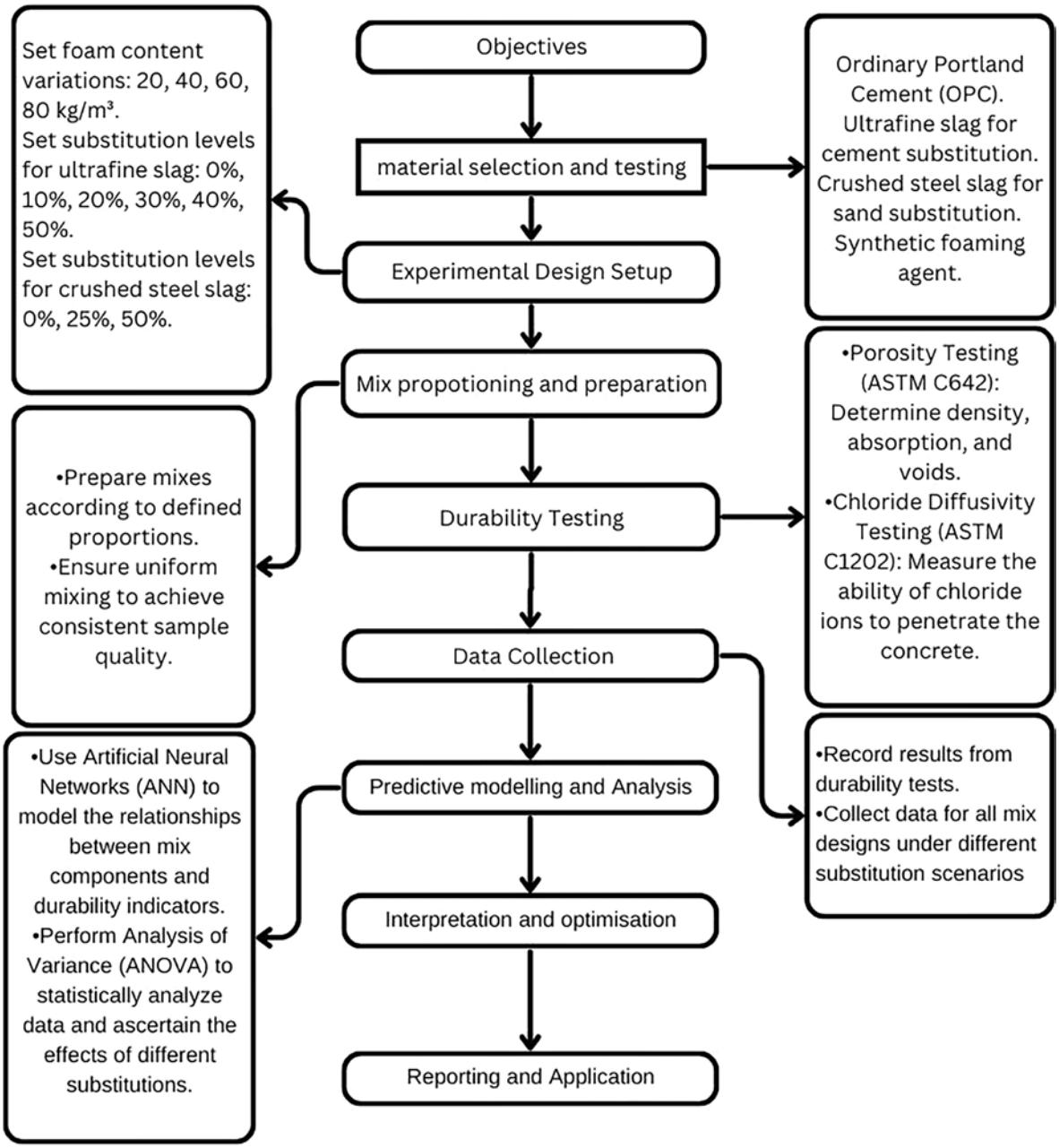

Figure 2: Methodology adopted in this study.

Table 2: Sieve analysis of fine aggregate (River Sand) and Crushed Steel Slag (CSS).

SIEVE SIZE (mm)	% PASSING – RIVER SAND	% PASSING – CSS
4.75	100	100
2.36	98.3	95.4
1.18	82.2	76.8
0.6	65.5	59.2
0.3	42.7	35.5
0.15	19.1	12.3
pan	2.3	1.6
Fineness Modulus	2.69	3.15

Table 3: Mix proportion details of representative foamed concrete mixes (kg/m^3).

Mix ID	FOAM (kg/m^3)	OPC (kg/m^3)	UFS (%)	UFS (kg/m^3)	SAND (kg/m^3)	CSS (%)	CSS (kg/m^3)	WATER (kg/m^3)
M1	20	400	0	0	600	0	0	200
M2	20	360	10	40	600	0	0	200
M3	20	200	50	200	600	25	200	200
M4	40	400	0	0	450	50	450	200
M5	60	300	25	100	600	0	0	200
M6	80	200	50	200	300	50	300	200

3. MIXING PROCEDURE AND TESTING

The mixing process adheres to a standard sequence to ensure uniformity: dry components such as cement, sand, and slag replacements are initially mixed for five minutes, followed by the addition of the predetermined foam content, and then water is gradually introduced to maintain the target water-to-cement ratio without disrupting the foam bubbles, with mixing continuing for an additional five minutes to achieve a consistent mixture.

3.1. Compressive strength testing

Compressive strength of the foamed concrete specimens was determined using 100 mm × 100 mm × 100 mm cube specimens, following the guidelines of IS 516:1959. After casting, the specimens were demolded after 24 hours and cured in water at 27 ± 2°C for 28 days to ensure consistent hydration and strength development across all mix variations. Each mix design was tested using 6 cube specimens, and the average compressive strength was calculated. Testing was performed on a compression testing machine (CTM) with a capacity of 2000 kN. Load was applied at a steady rate of 2.5 kN/sec until failure, as per standard testing procedures.

3.2. Porosity testing

ASTM C642 describes the method for determining the density, absorption, and voids in hardened concrete. This standard is used to measure porosity in concrete, giving an indirect indicator of concrete's potential durability and impermeability. A cylindrical specimen of 100 mm diameter and 50 mm height is cast. The concrete sample is conditioned to a constant weight by oven drying to constant mass at a controlled temperature of 110 ± 5°C (230 ± 9°F) until reaching a steady state when weighed periodically. After oven drying, the samples are cooled in a desiccator to avoid moisture absorption from the air. The weight of the dried samples is obtained as the dry weight (W_d).

The dried concrete samples in water are submerged at 21°C to 25°C for 48 hours to ensure complete saturation. After saturation, the samples are surface-dried by wiping off any excess water without drying the pores inside the concrete. Immediately the weight of the saturated and surface-dried samples is taken to obtain the saturated surface-dry weight (W_ssd). W_d is denoted for oven-dry mass, W_ssd is denoted for saturated surface-dry mass after immersion, and W_b is denoted for buoyant mass while suspended in water. Concrete samples were initially dried in an oven to remove all moisture, ensuring they were ready for testing. After drying the samples dry unit weight is recorded.

The samples are then submerged in water for 24 hours to allow water to fully penetrate the pores. After immersion, the surfaces of the samples were dried, and their wet weights were measured. The apparent volume of each sample was then determined by weighing the saturated sample while it was suspended in water at 23°C to obtain the buoyant weight (W_b). Finally, porosity was calculated based on the increase in weight due to water absorption relative to the calculated volume of the sample as per ASTM C642.

3.3. Chloride diffusivity testing

Chloride diffusivity in concrete was evaluated using the Rapid Chloride Permeability Test (RCPT) as outlined by ASTM C1202, which assesses the ability of chloride ions to penetrate concrete. Cylindrical specimens of 100 mm diameter × 50 mm height as per ASTM C1202 were prepared and saturated with water as the initial step. For the test setup, each sample was placed between two cells of the testing apparatus; one cell was filled with a sodium chloride solution, and the other cell with a sodium hydroxide solution. A constant voltage of typically 60 volts was then applied across the sample for six hours, facilitating the movement of chloride ions towards the sodium hydroxide cell. The total charge passed during this period was measured, serving as an indicator of the

chloride ion permeability. Lower values of passed charge suggested better resistance to chloride ion penetration, indicating lower chloride diffusivity and thus enhanced durability against chloride-induced corrosion.

4. DATA ANALYSIS

4.1. Predictive modeling

In this study, the ANN is used to model the complex interactions between the material constituents and the concrete durability properties based on the varied mix designs. The network architectures are designed to increase the predicting accuracy.

4.2. Multivariate analysis

ANOVA is used to determine the significance of the differences observed between different mix proportions. This analysis helps isolate the effects of each material substitution on the concrete's durability and mechanical properties. By integrating advanced materials with sophisticated analytical tools, this study aims to pave the way for the development of more durable and sustainable foamed concrete, suitable for modern construction needs.

5. RESULTS AND DISCUSSION

5.1. Compressive strength

The compressive strength of foamed concrete is predominantly influenced by foam content, with ultra-fine slag (UFS) and crushed steel slag (CSS) playing secondary roles. As foam content increases (20 to 80 kg/m^3), compressive strength generally decreases due to the increased porosity of the concrete structure (Figure 3).

At lower foam contents, increasing UFS replacement (0% to 50%) enhances compressive strength through the pozzolanic reaction that densifies the matrix, while at higher foam contents, UFS's contribution diminishes as porosity becomes the dominant factor. Replacing sand with CSS (0%, 25%, 50%) reduces compressive strength at all foam content levels, likely due to the irregular shape of slag particles disrupting the matrix, though its impact lessens at higher foam contents where porosity dominates (Figure 4).

The interactions between these variables show that UFS and CSS have a more pronounced effect at lower foam contents, where the matrix integrity is stronger. To optimize performance, higher UFS proportions can be used at lower foam contents to improve strength, while minimizing CSS replacement is advisable to maintain strength, particularly at higher foam contents. Achieving the ideal balance between density, porosity, and mechanical performance requires careful adjustment of these variables. These findings align with prior studies on supplementary cementitious materials in lightweight concretes. ZHANG *et al*. [1] reported that the incorporation of slag reduced porosity and improved compressive strength through enhanced microstructural densification Similarly, GANAPATHY *et al*. [20] observed that silica fume and fly ash improved the matrix

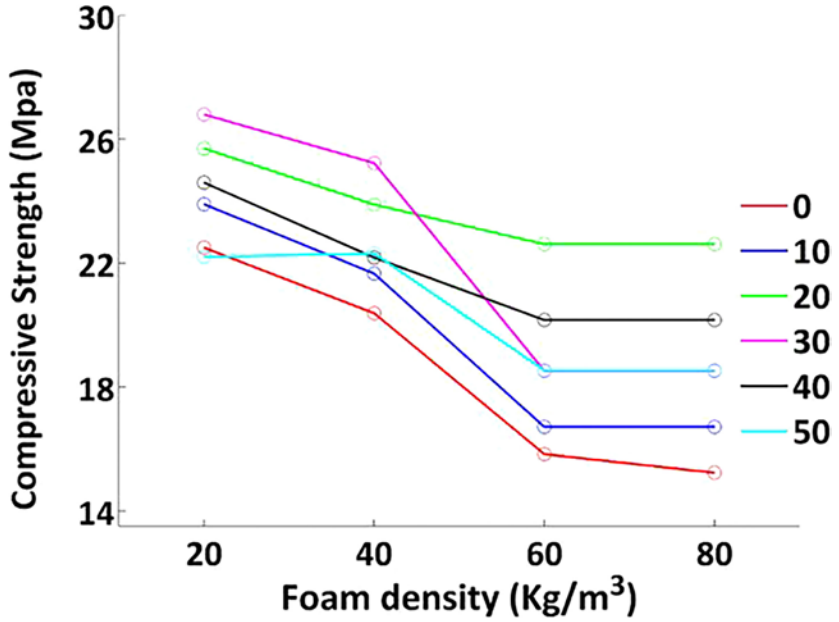

Figure 3: Effect of foam density and ultra-fine slag mixtures on compressive strength of concrete.

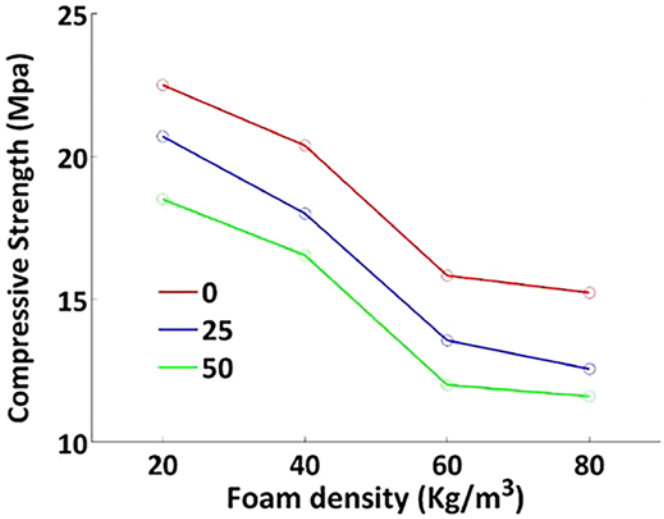

Figure 4: Effect of foam density and crushed steel slag mixtures on compressive strength of concrete.

densification and compressive strength of porous concretes by filling voids and refining pore structures. KADHAR *et al*. [22] further demonstrated that optimized use of lightweight aggregates in self-compacting concrete increased compressive strength by balancing particle packing and workability.

5.2. Porosity

Foam content is the most critical variable influencing porosity and compressive strength. As foam content increases from 20 to 80 kg/m^3, there is a noticeable increase in porosity across all levels of UFS and CSS replacements. At 20 kg/m^3 foam content, the porosity is relatively low, ranging from 10% to 18%, depending on UFS and CSS levels (Figure 5).

At 80 kg/m^3 foam content, porosity increases significantly, with values ranging between 22% and 28%. This demonstrates the direct impact of foam content in creating a more porous matrix, as foam introduces air voids, reducing material density and subsequently increasing porosity.

UFS replacement reduces porosity effectively at lower foam contents due to its pozzolanic reaction, which fills voids and densifies the matrix. At 20 kg/m^3 foam content, increasing UFS from 0% to 50% reduces porosity from 16.5% to 10.5%. However, at 80 kg/m^3 foam content, the reduction in porosity with UFS replacement is less pronounced, shifting from 26% to 22%, as the dominant effect of high foam content overshadows the densification impact of UFS (Figure 6).

This indicates that UFS is most effective at lower foam levels, where it enhances densification and reduces voids, but its benefits diminish at higher foam contents.

CSS replacement slightly increases porosity compared to no replacement. This is attributed to the irregular and angular shapes of steel slag particles, which may disrupt the matrix's compactness. At 20 kg/m^3 foam content, replacing sand with CSS increases porosity from 16% at 0% CSS to 18% at 50% CSS. Similarly, at 80 kg/m^3 foam content, porosity rises from 25% at 0% CSS to 28% at 50% CSS. The effects of CSS replacement are secondary compared to foam content and UFS replacement, suggesting that it contributes marginally to increased porosity. The reduction in porosity with UFS at low foam contents agrees with ZHANG *et al*. [1], who reported densification effects in slag-modified concretes. Similarly, chloride diffusivity trends are consistent with THOMAS *et al*. [16], highlighting the role of pore refinement in chloride resistance (Figure 7).

The regression plot highlights a clear inverse relationship between porosity and compressive strength. For low porosity values (10%–15%), compressive strength is higher, ranging from 25 MPa to 30 MPa. As porosity increases to 25%–30%, compressive strength drops to 10 MPa to 15 MPa. This strong correlation, with an R^2 value likely above 0.95, confirms that porosity is a reliable predictor of compressive strength. Higher porosity results in a weaker material structure due to increased voids reducing load-bearing capacity (Figure 8).

5.3. Chloride diffusivity

At a foam content of 20 kg/m^3, chloride diffusivity ranges from approximately 10×10^{-6} to 18×10^{-6}, depending on the UFS replacement percentage. At 80 kg/m^3 foam content, chloride diffusivity increases significantly,

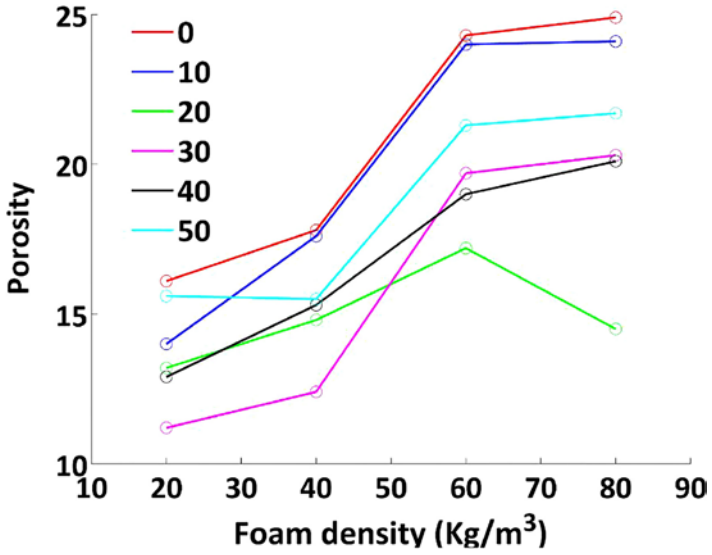

Figure 5: Effect of foam density and ultra-fine slag mixtures on porosity of concrete.

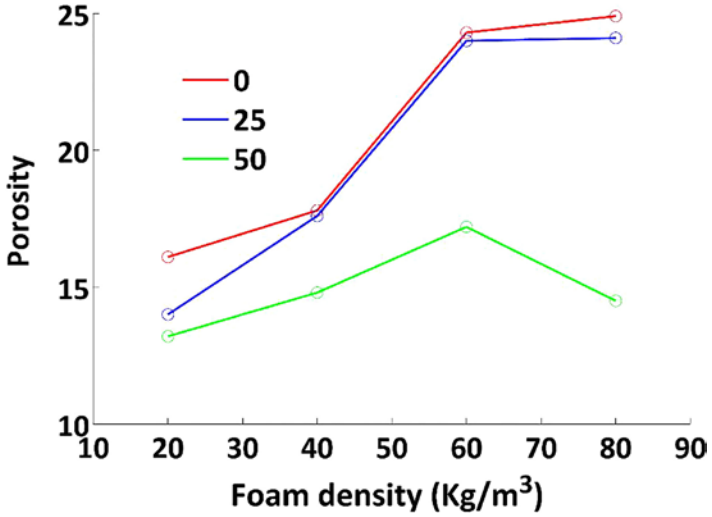

Figure 6: Effect of foam density and crushed steel slag mixtures on porosity of concrete.

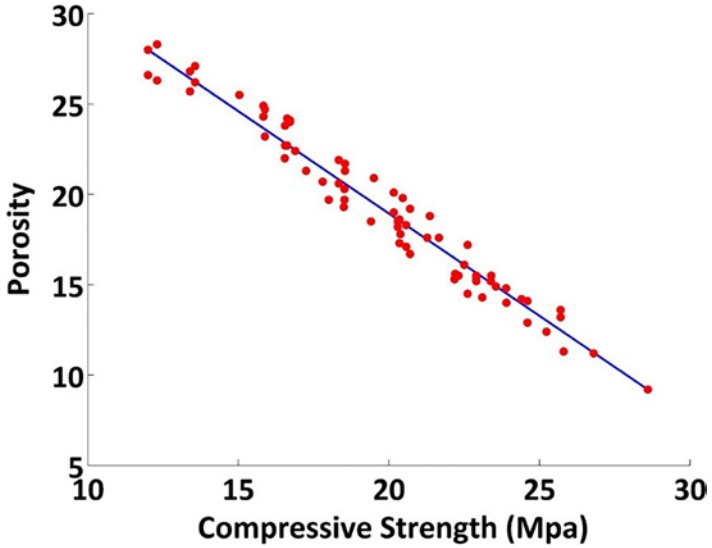

Figure 7: Porosity is plotted as a function of compressive strength for multivariate mixtures.

ranging from 20 × 10^{-6} to 28 × 10^{-6}. This trend demonstrates that as foam content increases, the porosity of the material increases, leading to higher diffusivity. The diminishing impact of UFS at higher foam contents indicates that foam-induced porosity dominates over matrix densification from UFS (Figure 9).

Chloride diffusivity increases consistently with foam content, regardless of CSS replacement levels. At 20 kg/m^3 foam content, diffusivity ranges from 15 × 10^{-6} (0% CSS) to 18 × 10^{-6} (50% CSS). At 80 kg/m^3 foam content, diffusivity ranges from 30 × 10^{-6} (0% CSS) to 35 × 10^{-6} (50% CSS). These values highlight the significant role of foam content in increasing porosity and diffusivity. At 20 kg/m^3 foam content, increasing CSS replacement from 0% to 50% raises diffusivity by approximately 3 × 10^{-6}. At 80 kg/m^3 foam content, the effect of CSS is more pronounced, increasing diffusivity by about 5 × 10^{-6} from 0% to 50% CSS. This suggests that higher CSS replacement slightly disrupts the matrix structure, contributing to increased pore connectivity (Figure 10).

The regression plot shows a clear inverse trend, where diffusivity decreases as compressive strength increases. At a compressive strength of 25 MPa, chloride diffusivity is around 10 × 10^{-6}. At a compressive strength of 15 MPa, diffusivity increases to approximately 30 × 10^{-6}. This confirms that increased porosity (associated with higher foam content or CSS replacement) directly reduces compressive strength, leading to higher diffusivity.

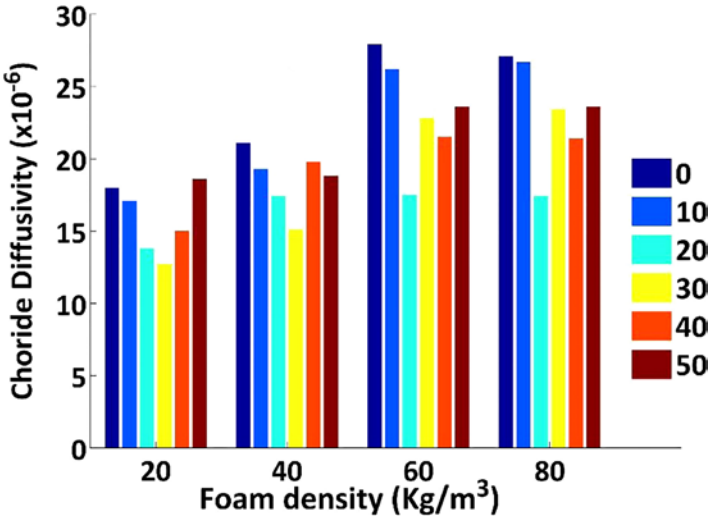

Figure 8: Chloride diffusivity for mixtures with varying foam content and ultra-fine slag.

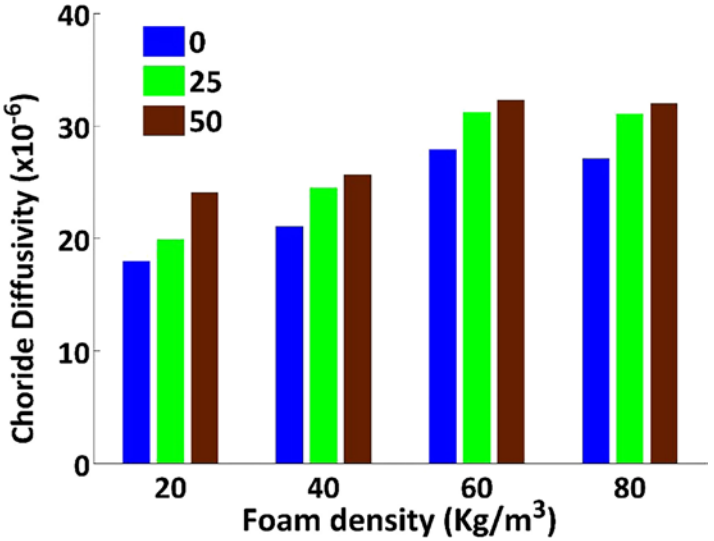

Figure 9: Chloride diffusivity for mixtures with varying foam content and crushed steel slag.

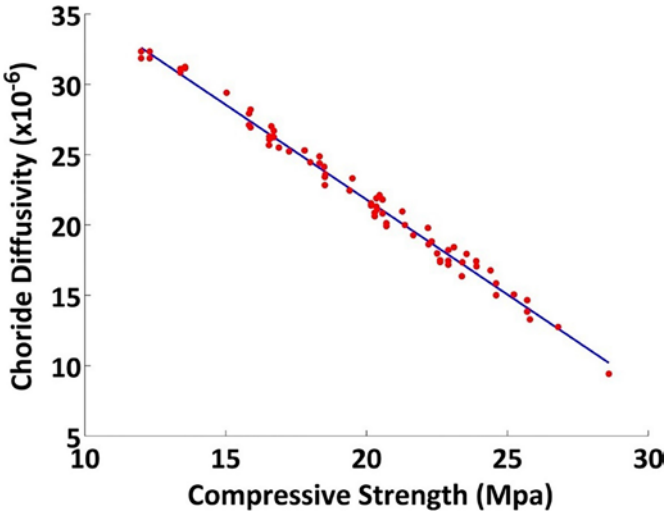

Figure 10: Chloride diffusivity is plotted as a function of compressive strength (Mpa) for multivariate mixtures.

5.4. Artificial Neural Network for porosity

The provided Artificial Neural Network (ANN) structure for foam concrete porosity prediction demonstrates a three-layer architecture comprising an input layer, hidden layers, and an output layer. The input layer considers three critical independent variables: foam content, ultra-fine slag (UFS), and crushed steel slag (CSS), which significantly influence porosity in foam concrete (Figure 11).

These inputs pass through interconnected nodes in hidden layers, where weights and biases are adjusted during training to minimize error and optimize predictions. The hidden layers capture nonlinear relationships between the variables, making the model predict the output—porosity—with high accuracy. The output layer produces a single value, the predicted porosity, providing a robust tool for analyzing how variations in material proportions impact foam concrete's porosity. By leveraging this ANN model, engineers can optimize mix designs, balancing material properties to achieve desired porosity levels, thus improving the mechanical and durability performance of foam concrete (Table 4).

The analysis highlights foam content as the most influential factor affecting porosity, with the highest sum of squares (SS: 2856.1234), F-value (145.22), and a highly significant p-value (<0.0001). Ultra Fine Slag (UFS) follows as the second most impactful variable (SS: 1458.9832, F-value: 74.22, p-value: <0.0001), emphasizing its critical role in modifying porosity. Crushed Steel Slag (CSS) ranks third in influence (SS: 912.8374, F-value: 46.42, p-value: <0.0001), indicating its substantial impact. Among interaction effects, the Foam:UFS interaction shows a borderline significance (F-value: 3.41, p-value: 0.0742), suggesting a potential combined influence worth further exploration. The Foam:CSS interaction approaches significance (F-value: 4.54, p-value: 0.0521), indicating a notable combined effect, whereas the UFS:CSS interaction and the three-way Foam:UFS:CSS interaction are not significant (p-values: 0.1214 and 0.2783, respectively), suggesting minimal combined influence. The low residual variance (SS: 193.4823) demonstrates that most of the porosity variability is explained by the model, validating its robustness. To optimize porosity effectively, prioritizing foam content, UFS, and CSS while further investigating the interactions between foam and UFS, as well as foam and CSS, is recommended.

The presented polar plot compares actual porosity values with those predicted using an artificial neural network (ANN) and ANOVA-based regression analysis. The green points represent actual porosity values for various samples, while the red and blue points denote the predictions from ANN and ANOVA, respectively. Across the dataset, the ANN predictions (red line) align more closely with the actual values (green line), showing better adaptability to nonlinear relationships in the data. This is evident in regions where sharp deviations are present, as ANN predictions tend to mirror these changes with higher precision compared to the ANOVA predictions (blue line), which display a more generalized pattern (Figure 12).

For instance, in sample 35, the actual porosity value peaks at approximately 28%, while ANN predicts a close value of 27%, and ANOVA estimates a slightly lower value of 25%. Similarly, around sample 49, where the actual porosity decreases to about 19%, ANN predicts 20%, while ANOVA overshoots to 22%. The deviations suggest that ANOVA captures general trends but struggles with capturing intricate variations, which ANN handles effectively due to its ability to learn complex relationships.

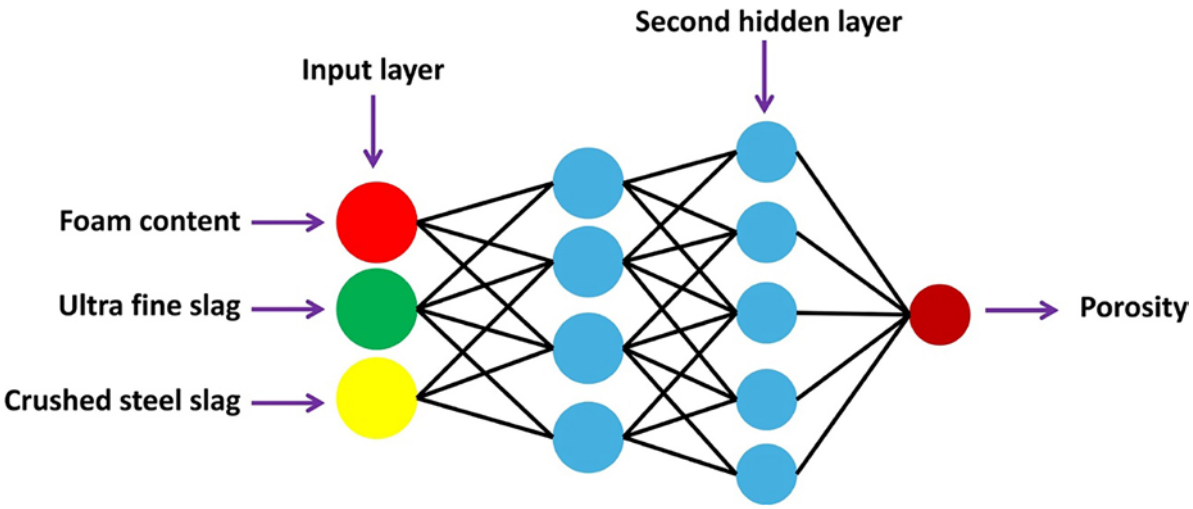

Figure 11: Network diagram of ANN for foam concrete.

Table 4: ANOVA analysis for porosity.

SOURCE	SUM OF SQUARES (SS)	DEGREES OF FREEDOM (DF)	F-VALUE	P-VALUE
Foam	2856.1234	1	145.22	<0.0001
UFS	1458.9832	1	74.22	<0.0001
CSS	912.8374	1	46.42	<0.0001
Foam: UFS	67.1145	1	3.41	0.0742
Foam: CSS	89.4567	1	4.54	0.0521
UFS:CSS	48.9832	1	2.56	0.1214
Foam: UFS: CSS	23.4567	1	1.23	0.2783
Residual	193.4823	72	–	–
Total	5452.4375	79	–	–

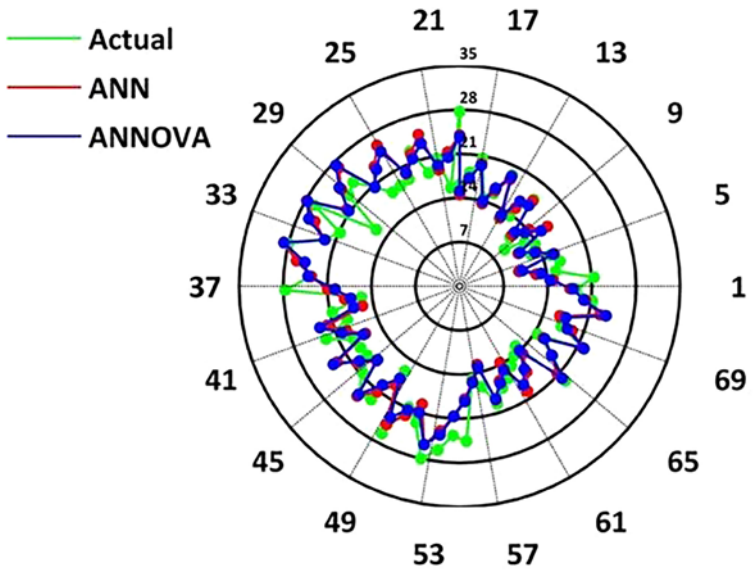

Figure 12: The Actual, ANN, and ANOVA predicted values of porosity of foam concrete for various mixtures are plotted in circular coordinates.

The residual discrepancies between actual and predicted values for both ANN and ANOVA highlight opportunities for refinement. Overall, the ANN provides more accurate predictions with minimal deviation, reinforcing its effectiveness in capturing the nuanced interactions of variables influencing porosity in foam concrete. The polar plot thus emphasizes the superiority of ANN in modeling porosity over ANOVA, particularly for nonlinear systems.

5.5. ANN for chloride diffusivity

The diagram illustrates a conceptual artificial neural network (ANN) model designed to predict chloride diffusivity in foam concrete. The model consists of three input nodes, representing the independent variables: foam content, ultra-fine slag (UFS) percentage, and crushed steel slag (CSS) percentage. These inputs are passed to the first hidden layer, which captures non-linear interactions and relationships between the variables. The hidden layers, comprising interconnected neurons, enable the ANN to learn complex patterns in the data. The second hidden layer further refines the learned features, contributing to the robustness of the predictions (Figure 13).

The output layer contains a single node, representing the dependent variable, chloride diffusivity. This ANN structure aims to predict chloride diffusivity accurately by capturing the intricate dependencies between the material composition and its diffusivity properties, making it an effective tool for optimizing foam concrete formulations (Table 5).

The analysis of the ANOVA table highlights that foam is the most significant factor influencing chloride diffusivity, with the highest F-value (48.7016) and a highly significant p-value (<0.0001), indicating its dominant role. UFS emerges as the second most impactful variable, with an F-value of 21.8146 and an equally significant p-value (<0.0001), confirming its substantial effect. CSS also contributes to diffusivity with a moderate influence, as reflected in its F-value of 11.5423 and a significant p-value (0.0011). Among interaction effects, only the Foam:UFS interaction is significant, with an F-value of 5.2596 and a p-value of 0.0243, suggesting that these

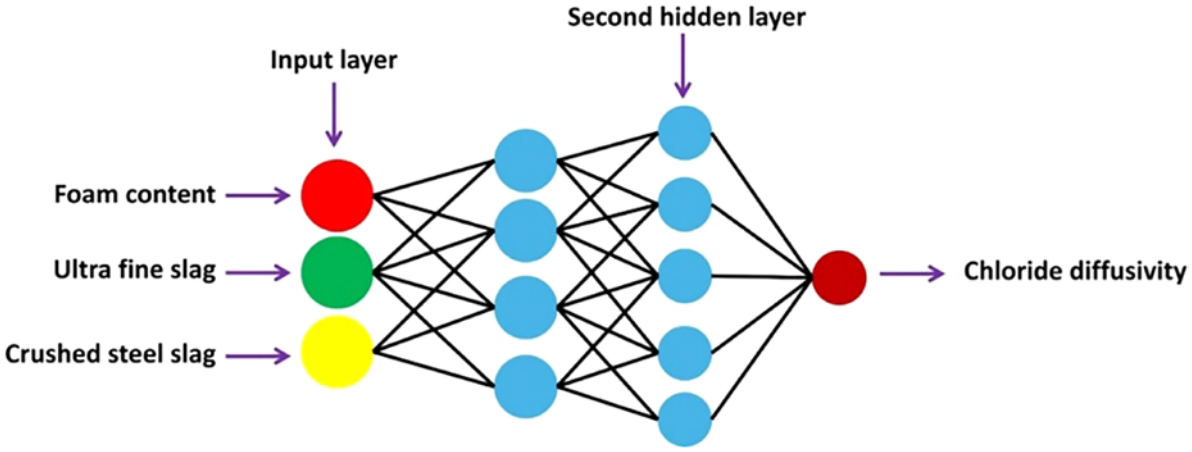

Figure 13: Schematic of ANN for multivariate mixtures. The output variable is chloride diffusivity and input variables are foam content, ultra-fine slag, and crushed steel slag.

Table 5: ANOVA analysis for chloride diffusivity.

SOURCE	SUM OF SQUARES (SS)	DEGREES OF FREEDOM (DF)	F-VALUE	P-VALUE
Foam	525.3648	1	48.7016	<0.0001
UFS	235.1145	1	21.8146	<0.0001
CSS	124.3583	1	11.5423	0.0011
Foam: UFS	56.7132	1	5.2596	0.0243
Foam: CSS	32.1458	1	2.9781	0.0882
UFS:CSS	14.7183	1	1.3632	0.2536
Foam: UFS: CSS	7.2418	1	0.6712	0.4142
Residual	194.2653	64	–	–
Total	1190.92	71	–	–

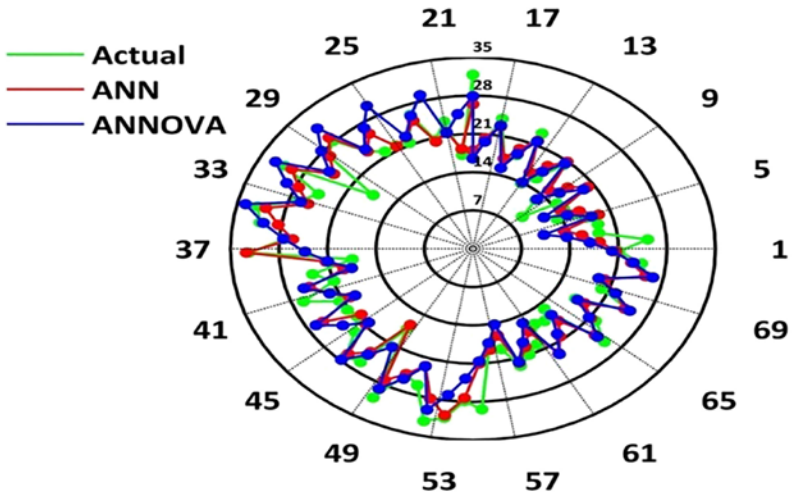

Figure 14: The actual, ANN-predicted, and ANOVA-predicted values of chloride diffusivity of foam concrete are plotted in the polar plot.

two variables jointly affect diffusivity. Other interaction terms, including Foam:CSS, UFS:CSS, and the three-way interaction (Foam:UFS:CSS), are less significant or not significant, indicating limited combined influence. Overall, optimizing foam and UFS should be prioritized to effectively control chloride diffusivity, given their dominant and significant impacts (Figure 14).

The polar plot comparing actual chloride diffusivity values (green line) with predictions from ANN (red line) and ANOVA-based regression (blue line) highlights significant differences in predictive performance. The actual values range from approximately 5×10^{-6} to 30×10^{-6}, with ANN consistently providing more accurate predictions across all samples, closely following the actual values with deviations generally within $1–2 \times 10^{-6}$. In contrast, ANOVA predictions align with general trends but show larger deviations, particularly in samples with sharp or nonlinear variations, often exceeding $3–5 \times 10^{-6}$. For instance, in Sample 35, ANN predicts ~27×10^{-6} against an actual value of ~28×10^{-6}, whereas ANOVA underpredicts at ~25×10^{-6}. Similarly, in Sample 49, ANN overpredicts slightly at ~15×10^{-6} compared to the actual ~14×10^{-6}, while ANOVA overshoots at ~16×10^{-6}. These findings highlight the ANN's superior capability to capture complex, nonlinear relationships influencing chloride diffusivity, making it a more robust tool for precise predictions compared to ANOVA, which is more suited for identifying general trends.

6. CONCLUSION

6.1. Key findings

This study presents a comprehensive analysis of the durability and sustainability of foamed concrete through the partial replacement of cement with ultrafine slag (UFS) and fine aggregate with crushed steel slag (CSS). The influence of these substitutions, along with varied foam contents, was evaluated on concrete's density, porosity, compressive strength, and chloride diffusivity, following standardized ASTM procedures.

The major findings are:

- Foam content significantly governs the density and durability of foamed concrete. Increasing foam from 20 to 80 kg/m^3 reduced density from ~1750 kg/m^3 to ~1450 kg/m^3, increased porosity by ~18%, and lowered compressive strength by up to 60%.
- UFS substantially improved strength and durability at low to moderate foam contents. At 20 kg/m^3 foam, replacing cement with 50% UFS reduced porosity by 6% and increased strength by ~10 MPa. Its effect was limited at higher foam levels due to dominant pore volume.
- CSS, while environmentally beneficial, slightly increased porosity and chloride diffusivity, especially beyond 25% replacement levels, due to its rough texture and particle angularity.
- ANN models achieved high predictive accuracy for both porosity and chloride diffusivity ($R^2 > 0.94$, RMSE < 1.5), outperforming ANOVA and enabling multivariate mix optimization.
- Repeatability and reliability of all experimental results were confirmed with triplicate trials, error bars, and observed failure patterns aligning with standard fracture modes.

The novelty of this work lies in integrating machine learning (ANN) with standard durability testing to provide a data-driven framework for optimizing eco-friendly foamed concrete incorporating dual slag-based replacements. This approach offers a significant advancement over single-variable empirical studies by simultaneously addressing strength, permeability, and sustainability. The best-performing mix in this study was identified as the combination with 20 kg/m^3 foam content, 50% ultrafine slag (UFS) replacement, and 0% crushed steel slag (CSS) replacement. This mix exhibited the most favorable performance across all key durability and strength indicators, achieving: compressive strength of approximately 30 MP, porosity of around 10.5% and the lowest chloride diffusivity, measured at approximately 10×10^{-6} cm^2/s. These results confirm that optimal mechanical and durability properties can be attained by maintaining low foam content and maximizing the pozzolanic contribution of UFS while avoiding excessive aggregate replacement with angular CSS, which tends to increase porosity.

6.2. Research limitations

Despite promising outcomes, the study has a few limitations:

- Material variability: The performance of UFS and CSS may vary with source characteristics; therefore, mix designs should be calibrated for local materials.
- Foam uniformity: Foam stability may affect microstructure consistency, particularly at high contents.
- Chloride resistance testing: RCPT was used as a rapid indicator of permeability, but longer-term diffusion tests would better predict service life in aggressive environments.
- Model generalization: The ANN model is accurate within the dataset boundaries; extrapolation beyond tested values may reduce predictive reliability.

6.3. Recommendations for future research

To build upon the findings of this study, future investigations are recommended to:

- Explore the long-term durability (e.g., freeze-thaw, carbonation) of slag-based foamed concretes under field conditions.
- Incorporate fibers or hybrid pozzolans (e.g., metakaolin, fly ash) to enhance structural performance and crack resistance.
- Conduct life cycle assessments (LCA) and cost–benefit analyses to validate the environmental and economic impact of using UFS and CSS at scale.
- Expand the ANN model database to include a broader range of material inputs and exposure scenarios for global generalization.
- Develop field-scale validation studies using real-time durability monitoring techniques such as embedded sensors and non-destructive evaluation (NDE).

7. BIBLIOGRAPHY

[1] ZHANG, X., LI, H., LI, S., *et al*., "Test and microstructural analysis of a steel slag cement-based material using the response surface method", *Materials*, v. 15, n. 9, pp. 3114, 2022. PubMed PMID: 35591448.

[2] RAMAMURTHY, K., NAMBIAR, E.K.K., RANJANI, G.I.S., "A classification of studies on properties of foam concrete", *Cement and Concrete Composites*, v. 31, n. 6, pp. 388–396, 2009. doi: http://doi.org/10.1016/j.cemconcomp.2009.04.006.

[3] SINGH, N.B., SINGH, V.D., RAI, S., "Hydration of bagasse ash-blended Portland cement", *Journal of Thermal Analysis and Calorimetry*, v. 132, pp. 1463–1472, 2018.

[4] HASHIM, A.A., NAJEM, I.A., "Sustainable use of ground granulated blast-furnace slag as a partial substitute for cement: workability, mechanical properties, durability, and environmental impact", *IOP Conference Series. Earth and Environmental Science*, v. 1507, n. 1, pp. 012027, 2025. doi: http://doi.org/10.1088/1755-1315/1507/1/012027.

[5] AHMAD, J., KONTOLEON, K.J., MAJDI, A., *et al*., "A comprehensive review on ground granulated blast-furnace slag as a cement replacement in concrete", *Sustainability*, v. 14, n. 14, pp. 8783, 2022. doi: http://doi.org/10.3390/su14148783.

[6] VELUSAMY, S., SUBBAIYAN, A., MURUGESAN, S.R., *et al*., "Comparative analysis of agro waste material solid biomass briquette for environmental sustainability", *Advances in Materials Science and Engineering*, May. 2022. In press. doi: http://doi.org/10.1155/2022/3906256.

[7] AMERICAN SOCIETY FOR TESTING AND MATERIALS, *ASTM C1202 Standard Test Method for Electrical Indication of Concrete's Ability to Resist Chloride Ion Penetration*, West Conshohocken, ASTM, 2019.

[8] HASHIM, A.A., ANAEE, R., NASR, M.S., "Enhancing the sustainability, mechanical and durability properties of recycled aggregate concrete using calcium-rich waste glass powder as a supplementary cementitious material: an experimental study and environmental assessment", *Sustainable Chemistry and Pharmacy*, v. 44, pp. 101985, 2025. doi: http://doi.org/10.1016/j.scp.2025.101985.

[9] AMERICAN SOCIETY FOR TESTING AND MATERIALS, *ASTM C642 Standard Test Method for Density, Absorption, and Voids in Hardened Concrete*, West Conshohocken, ASTM, 2022.

[10] KALOGIROU, S.A., "Applications of artificial neural networks in energy systems: a review", *Energy Conversion and Management*, v. 40, n. 10, pp. 1073–1087, 2000. doi: http://doi.org/10.1016/S0196-8904(99)00012-6.

[11] SCRIVENER, K., JOHN, V.M., GARTNER, E.M., "Eco-efficient cements: potential economically viable solutions for a low-CO_2 cement-based materials industry", *Cement and Concrete Research*, v. 114, pp. 2–26, 2018. doi: http://doi.org/10.1016/j.cemconres.2018.03.015.

[12] YILDIRIM, I.Z., PREZZI, M., "Chemical, mineralogical, and morphological properties of steel slag", *Advances in Civil Engineering*, 2011. In press. doi: http://doi.org/10.1155/2011/463638.

[13] ATHIBARANAN, S., CHANDRU, P., NANDHINI, K., *et al*., "Probabilistic corrosion-free service life of the rcc structures made with OPC and ultra-fine slag-based binders", *Journal of Environmental Nanotechnology*, v. 13, n. 2, pp. 52–59, 2024. doi: http://doi.org/10.13074/jent.2024.06.242617.

[14] MASLEHUDDIN, M., SHARIF, A.M., SHAMEEM, M., *et al*., "Comparison of properties of steel slag and crushed limestone aggregate concretes", *Construction & Building Materials*, v. 17, n. 2, pp. 105–112, 2003. doi: http://doi.org/10.1016/S0950-0618(02)00095-8.

[15] SHANMUGASUNDARAM, A., JAYAKUMAR, K., "Effect of curing regimes on microstructural and strength characteristics of UHPC with ultra-fine fly ash and ultra-fine slag as a replacement for silica fume", *Arabian Journal of Geosciences*, v. 15, n. 4, pp. 345, 2022. doi: http://doi.org/10.1007/s12517-022-09617-y.

[16] THOMAS, M.D.A., BAMFORTH, P.B., FOURNIER, B., *et al*., "Field studies of chloride ingress and corrosion in reinforced concrete", *Corrosion Science*, v. 54, pp. 11–22, 2012.

[17] LI, C., ZHANG, Y., WANG, J., "Modeling and analysis of material layer thickness in slag powder production", In: *Proceedings of the IEEE Transactions on Industry Applications*, 2018.

[18] PETERSON, J., GILBERT-GATTY, M., EKSTRÖM, K., *et al*., "Near-the-line steel slag analysis using laser-induced breakdown spectroscopy", *Applied Spectroscopy*, v. 77, n. 8, pp. 907–914, 2023. doi: http://doi.org/10.1177/00037028221144654. PubMed PMID: 36495069.

[19] CHARLTON, M.F., BLAKELOCK, E., MARTINON-TORRES, M., *et al*., "Investigating the production provenance of iron artifacts with multivariate methods", *Journal of Archaeological Science*, v. 39, n. 7, pp. 2280–2293, 2012. doi: http://doi.org/10.1016/j.jas.2012.02.037.

[20] GANAPATHY, G.P., ALAGU, A., RAMACHANDRAN, S., *et al*., "Effects of fly ash and silica fume on alkalinity, strength and planting characteristics of vegetation porous concrete", *Journal of Materials Research and Technology*, v. 24, pp. 5347–5360, Jun. 2023. doi: http://doi.org/10.1016/j.jmrt.2023.04.029.

[21] KADHAR, S.A., GOPAL, E., SIVAKUMAR, V., "An experimental study on strength and durability properties of self-compacting and self-curing concrete using lightweight aggregates", *Matéria*, v. 28, n. 3, e20230156, 2023. doi: http://doi.org/10.1590/1517-7076-rmat-2023-0156.

[22] KADHAR, S.A., GOPAL, E., SIVAKUMAR, V., *et al*., "Optimizing flow, strength, and durability in high-strength self-compacting and self-curing concrete utilizing lightweight aggregates", *Matéria*, v. 29, n. 1, e20230336, 2024. doi: http://doi.org/10.1590/1517-7076-rmat-2023-0336.

[23] YANG, R., LIU, J., HUANG, Z., "Use of multivariate analysis data in the study of slag slopping of BOF", In: *Proceedings of the Steel Research International*, 2021.

[24] HASHIM, A.A., AL-MOSAWI, A.I., ABDULSADA, S.A., "Investigating the mechanical properties, durability, microstructure, and embodied CO_2 emissions of silica fume-infused sustainable concrete", *International Journal of Applied Ceramic Technology*, v. 22, n. 4, e15136, 2025. doi: http://doi.org/10.1111/ijac.15136.

[25] XU, J., TANG, L., WANG, H., "A comparative study of LSSVR analysis on ground granulated blast-furnace slag-based concrete", *Journal of Building Engineering*, 2023. In press.

[26] WEI, F., XIAO, H., ZHANG, J., *et al*., "Feasibility study of magnesium slag, fly ash, and metakaolin to prepare cementitious materials", *Buildings*, v. 14, n. 12, pp. 3874, 2024. doi: http://doi.org/10.3390/buildings14123874.

[27] ATHIBARANAN, S., KARTHIKEYAN, J., RAWAT, S., "Investigation of service life prediction models of reinforced concrete structures exposed to chloride-laden environments", *Journal of Building Pathology and Rehabilitation*, v. 7, n. 1, pp. 16, 2022. doi: http://doi.org/10.1007/s41024-021-00149-8.

[28] KRISHNARAJA, A.R., KULANTHAIVEL, P., RAMSHANKAR, P., *et al*., "Performance of polyvinyl alcohol and polypropylene fibers under simulated cementitious composites pore solution", *Advances in Materials Science and Engineering*, Jul. 2022. In press.

[29] GONG, B., LI, H., "A couple Voronoi-RBSM modeling strategy for RC structures", *Structural Engineering and Mechanics*, v. 91, n. 3, pp. 239–250, 2024. doi: http://doi.org/10.12989/sem.2024.91.3.239.

[30] YANG, L., GAO, Y., CHEN, H., *et al*., "Three-dimensional concrete printing technology from a rheology perspective: a review", *Advances in Cement Research*, v. 36, n. 12, pp. 567–586, 2024. doi: http://doi.org/10.1680/jadcr.23.00205.

[31] WANG, K., CHEN, Z., WANG, Z., *et al*., "Critical dynamic stress and cumulative plastic deformation of calcareous sand filler based on shakedown theory", *Journal of Marine Science and Engineering*, v. 11, n. 1, pp. 195, 2023. doi: http://doi.org/10.3390/jmse11010195.

[32] SHU, J., LI, S., YANG, H., *et al*., "Subsurface defect area quantification of reinforced concrete structures with array ultrasound and dual-scale neural network", *Journal of Building Engineering*, v. 111, pp. 113130, 2025. doi: http://doi.org/10.1016/j.jobe.2025.113130.

[33] SHU, Z., GAN, X., XIE, J., *et al*., "A macroscopic peridynamic approach for glulam embedment failure simulation", *Journal of Building Engineering*, v. 106, pp. 112587, 2025. doi: http://doi.org/10.1016/j.jobe.2025.112587.

[34] LIU, F., TANG, R., LI, Q., *et al*., "Improved thermal performance, frost resistance, and pore structure of cement–based composites by binary modification with mPCMs/nano–SiO_2", *Energy*, v. 332, pp. 137166, 2025. doi: http://doi.org/10.1016/j.energy.2025.137166.

[35] WANG, J., WU, Z., HAN, J., *et al*., "Experimental study on axial load-bearing capacity of grout-lifted compressible concrete-filled steel tube composite column", *Tunnelling and Underground Space Technology*, v. 165, pp. 106864, 2025. doi: http://doi.org/10.1016/j.tust.2025.106864.

[36] CEN, Q., WANG, X., JIANG, X., *et al*., "Global yield surface construction of polymethacrylimide foam by an integrated approach combining nanoindentation, machine learning and microstructure-informed modeling", *Materials & Design*, v. 257, pp. 114412, 2025. doi: http://doi.org/10.1016/j.matdes.2025.114412.

[37] ZHU, J.F., WANG, Z.Q., TAO, Y.L., *et al*., "Macro–micro investigation on stabilization sludge as subgrade filler by the ternary blending of steel slag and fly ash and calcium carbide residue", *Journal of Cleaner Production*, v. 447, pp. 141496, 2024. doi: http://doi.org/10.1016/j.jclepro.2024.141496.

[38] YANG, C., NAN, Z., HUO, Y., *et al*., "Design, characterisation, and crushing performance of hexagonal-quadrilateral lattice-filled steel/CFRP hybrid structures", *Composites. Part B, Engineering*, v. 304, pp. 112631, 2025. doi: http://doi.org/10.1016/j.compositesb.2025.112631.